Early cardiac remodeling in aortic coarctation: insights from fetal and neonatal functional and structural assessment

Iris Soveral[a], MD, Fatima Crispi*[a], MD, PhD, Carin Walter[b], MD, Laura Guirado[a], MD, Patricia García-Cañadilla[c,d], PhD, Andrew Cook[d], PhD, Anne Bonnin[e], PhD, Hector Dejea[e,f], MSc, Carlota Rovira-Zurriaga[g], MD, Joan Sánchez de Toledo[b], MD, PhD, Eduard Gratacós[a], MD, PhD, Josep Maria Martínez[a], MD, PhD, , Bart Bijnens†[c,h] PhD, Olga Gómez†[a], MD, PhD.

a. Fetal i+D Fetal Medicine Research Center, BCNatal - Barcelona Center for Maternal-Fetal and Neonatal Medicine (Hospital Clínic and Hospital Sant Joan de Déu), Institut Clínic de Ginecologia Obstetricia i Neonatologia, Institut d'Investigacions Biomèdiques August Pi i Sunyer, Universitat de Barcelona, Centre for Biomedical Research on Rare Diseases (CIBER-ER), C/Sabino Arana 1, 08028 Barcelona, Spain.
b. Pediatric Cardiology, Hospital Sant Joan de Déu, Passeig de Sant Joan de Déu, 2, 08950 Esplugues de Llobregat, Barcelona, Spain
c. PhySense, DTIC, Universitat Pompeu Fabra, Plaça de la Mercè, 10, 08002 Barcelona, Spain
d. Institute of Cardiovascular Science, University College London, Gower St, Bloomsbury, London WC1E 6BT, UK
e. Swiss Light Source, Paul Scherrer Institut, Forschungsstrasse 111, 5232 Villigen, Switzerland
f. Institute for Biomedical Engineering, ETH Zürich, Gloriastrasse 35, 8092 Zürich, Switzerland
g. Department of Pathology, Hospital Sant Joan de Déu, Passeig de Sant Joan de Déu, 2, 08950 Esplugues de Llobregat, Barcelona, Spain
h. ICREA, Passeig Lluís Companys 23, 08010 Barcelona, Spain

*Corresponding author
† Both last authors contributed equally to the study.

***Adress for correspondence:**
Fàtima Crispi,
Fetal i+D Fetal Medicine Research Center, BCNatal- Barcelona Center for Maternal-fetal and Neonatal Medicine (Hospital Clínic and Hospital Sant Joan de Déu).
Sabino de Arana street 1, 08028, Barcelona, Spain.
E-mail: fcrispi@gmail.com/

Short title: Early cardiac remodeling in aortic coarctation

Keywords: aortic coarctation, fetal cardiac function, neonatal cardiac function, echocardiography, synchrotron tomography

This article has been accepted for publication and undergone full peer review but has not been through the copyediting, typesetting, pagination and proofreading process which may lead to differences between this version and the Version of Record. Please cite this article as doi: 10.1002/uog.21970

CONTRIBUTION

What are the novel findings of this work?

This study provides a comprehensive assessment of biventricular morphometry and function in CoA and offers new insights on cardiovascular adaptation as fetuses with CoA transition to the neonatal circulation.

What are the clinical implications of this work?

Our findings highlight the importance of the neonatal period as a critical time in which a previously normal functioning heart must rapidly accommodate a volume overload for which it seems poorly adapt. Thus, the neonatal period might provide an opportunity to deploy strategies that minimize adverse LV remodeling.

ABSTRACT

Objective: Coarctation of the aorta (CoA) is associated with left ventricular (LV) dysfunction in neonates and adults; however cardiac structure and function in fetal CoA and the neonatal cardiac adaptation has not been described. We aimed to investigate the presence of cardiovascular structural remodeling and dysfunction in fetuses with CoA and their early postnatal cardiac adaptation.

Methods: A prospective observational case-control study was conducted in 30 fetuses with CoA and 60 gestational-age matched normal controls. A comprehensive echocardiographic evaluation was performed at third trimester of pregnancy and after birth (20 CoA and 44 controls). Additionally, myocardial microstructure was assessed in one fetus and one neonatal CoA, using synchrotron-based phase-contrast X-ray tomography and histology, respectively.

Results: Fetuses with CoA showed significant left-to-right volume redistribution with right ventricular (RV) size and output dominance and significant geometry alterations with an abnormally elongated left ventricle (LV) (LV sphericity: CoA median 2.4 (IQR 0.7) vs. controls 1.8 (0.4)*, p<0.001*). Biventricular function was preserved, and no ventricular hypertrophy was observed. Synchrotron tomography and histological assessment revealed normal myocyte organization. Postnatally, the LV showed prompt remodeling becoming more globular (LV sphericity: CoA 1.5 (0.4) vs. controls 1.8 (0.3), *p<0.001*) with preserved systolic and normalized output, but altered diastolic parameters (LV E-wave velocity 97.0 (55.0) vs. 57.0 (16.0) cm/s; A-wave velocity 70.5 (24.8) vs. 47.0 (12.0) cm/s; A' 4.8 (5.1) vs. 6.0 (3.0) cm/s; p<0.05). The neonatal RV showed increased longitudinal function in the presence of a patent arterial duct.

Conclusions:

Our results suggest a unique fetal cardiac remodeling in which the LV stays smaller from the decreased growth stimulus of reduced volume load. Postnatally, the LV is acutely volume loaded resulting in an overall geometry change with higher filling velocities and preserved systolic function. These findings improve our understanding of CoA from fetal to neonatal life.

INTRODUCTION

Coarctation of the aorta (CoA) accounts for 6-8% of congenital heart defects (CHD) and is defined as narrowing of the aortic isthmus and, to a variable degree, the aortic arch[1]. Advances in prenatal diagnosis have contributed to significantly reduce neonatal morbi-mortality of CoA in the last decades[2]. However, prenatal detection remains challenging as it relies on indirect signs of cardiovascular remodeling within the complexity of the fetal circulation[3]. Thus, most studies focused on describing the right heart dominance and identifying related parameters that improve diagnostic accuracy but there is very little information on cardiac functional changes and it is not clear whether fetuses with CoA present intrinsic myocardial dysfunction[4,5].

Cardiac remodeling manifests clinically as changes in size, mass, geometry and function of the heart in response to load or injury[6]. This process can lead to impaired cardiac relaxation and/or ejection ability, which translates into clinical or subclinical dysfunction. Cardiac structural remodeling and dysfunction have been in a variety of prenatal conditions[7–9], however this information is scarce in fetuses with CHD[10].

Such a comprehensive structural and functional evaluation in CoA could improve prenatal diagnosis and counseling and our understanding of the neonatal biventricular response. In this regard, biventricular dysfunction in neonates prior to surgical treatment -with a pharmacologically open arterial duct- has been described[11]. Additionally, persistent left ventricular (LV) alterations[12] and increased cardiovascular risk, regardless of the presence of

hypertension[13], has been reported in both children and adults with repaired CoA. Whether these alterations are present prenatally and result from abnormal fetal myocardial differentiation or are the result of postnatal cardiovascular remodeling remains to be clarified. Cardiac tissue microstructural analysis could shed light on this issue but no data on myocardial microscopic characteristics of CoA has been reported in the human fetus. New techniques, such as synchrotron radiation-based X-ray phase-contrast micro computed tomography (X-PCI), show great promise in the assessment of whole heart cardiac microstructure, without the difficulties of classic histology[14,15].

The aim of the present study was to investigate the presence of cardiovascular structural remodeling and dysfunction in fetuses with CoA and to describe early postnatal cardiac adaptation.

METHODS

Study population

This study was approved by the institutional Ethics Committee and written informed consent was obtained from all patients.

This prospective observational case-control study was conducted between 2011-2018 in a tertiary referral center for fetal and pediatric CHD (Hospital Clinic and Sant Joan de Déu) in Barcelona. Cases were selected from fetuses with high echocardiographic suspicion of CoA (significant right dominance and aortic isthmus diameter < - 2 z-score)[3] evaluated in our center during the study period. Exclusion criteria included pre or postnatal diagnosis of additional major cardiac malformations (including LV outflow tract obstruction or mitral valve disease within Shone Complex), major extra cardiac malformations and genetic anomalies. The presence of bicuspid aortic valve was not considered an exclusion criterion unless it resulted in LV outflow obstruction neither was the presence of minor cardiovascular anomalies including ventricular septal defects.

For each case, we recruited two gestational age (GA) matched controls among patients visited at our center for routine pregnancy ultrasound scans. Only single uncomplicated spontaneously conceived pregnancies without known maternal or gestational conditions potentially affecting cardiovascular remodeling were selected. GA was calculated based on the crown-rump length obtained at first trimester ultrasound[16]. Third trimester fetal (32 to 36 weeks gestation) echocardiography and measurements were performed by experienced fetal medicine specialists (IS, LG, FC and OF). Early neonatal (48-96 hours after birth) echocardiography and measurements were performed by an experienced pediatric cardiologist (CW). To eliminate potential confounders, only term neonates (>37 weeks), both cases and controls, with complete echocardiographic assessment performed between 48-96

hours after birth and prior to coarctation treatment were included in the postnatal analysis. Additionally, for CoA cases we chose to include only those under prostaglandin E1 treatment. No controls were treated with PGE1.

Cardiac histopathology was assessed in one case, corresponding to a preterm (32.4 weeks) newborn with CoA. Furthermore, the database of the Cardiac Archive at the Institute of Cardiovascular Science and Child Health held under license of the UK Human Tissue Authority was searched to find whole human fetal heart specimens with isolated CoA. Only one specimen with these characteristics was found corresponding to a 19 weeks fetus. We, then, searched the database for one whole normal heart specimen of similar gestational age. X-PCI was then performed on both 19 weeks human fetal heart specimens, one with CoA and one normal heart.

Maternal and perinatal characteristics

Maternal characteristics, co-morbidities and gestational complications were obtained from interview and medical records. Standard obstetric ultrasound and fetal echocardiography were performed at the third trimester, using a Siemens Sonoline Antares (Siemens Medical Systems, Malvern, PA, USA) with a curved-array 2-6 MHz and 2-10 MHz. Fetal ultrasound followed recommended guidelines and included estimated fetal weight and centile, extra-cardiac and cardiac detailed examinations[17] and umbilical and middle cerebral arteries pulsatility index[18]. Fetal weight was estimated according to Hadlock et al.[19] and estimated fetal weight centile was calculated using local reference curves[20]. Delivery characteristics included GA at delivery, mode of delivery, Apgar score, umbilical artery pH, birth weight and centiles[20]. Data regarding additional minor cardiovascular anomalies, age at scan and neonatal intensive

care admission was collected. For CoA cases, PGE1 treatment, type of surgery, age at surgery, hospitalization stay, and post-operative complications were also obtained.

Fetal echocardiography

Fetal echocardiography was performed using a Siemens Sonoline Antares (Siemens Medical Systems, Malvern, PA, USA) with a curved-array 2-6 MHz and 2-10 MHz. *Fetal cardiac morphometric* measurements included cardiac and thoracic areas, cardiac longitudinal and transverse diameters, right (RV), left ventricular diameters (longitudinal, atrio-ventricular valves (basal and mid-transverse) and septal and ventricular wall thickness[21]. Cardiothoracic ratio, cardiac sphericity, right-to-left ratios and ventricular sphericity indexes were calculated. Fetal cardiac morphometric measurements were obtained from a 2 dimensional apical or basal 4-chamber view at end-diastole, unless otherwise specified. Cardiothoracic ratio was obtained dividing cardiac by thoraric area[22]. Cardiac sphericity and ventricular sphericity indexes were calculated dividing longitudinal by transverse diameters. Atrial areas were measured at end-systolic maximum distention point by manual area delineation. Ventricular dimensions (longitudinal, atrio-ventricular valves (basal) and mid-transverse) were measured following previously published guidelines[23]. Diameters of the pulmonary and aortic valves were measured during systole as previously decribed[23]. Right and left ventricular end-diastolic septal and free wall thicknesses were measured by M mode from a transverse 4-chamber view[24]. Right to left ratios were calculated dividing right by left measurements.

Systolic function evaluation[25] included heart rate (HR), RV fractional area change (FAC), right and left stroke volumes (SV), cardiac output (CO), LV shortening fraction (SF), tricuspid (TAPSE) and mitral (MAPSE) annular-plane systolic excursion, peak systolic myocardial velocities (S') and ejection times. Heart rate was calculated from the spectral

Doppler of aortic and pulmonary flow, averaging 3 cardiac cycles. RV areas were measured by manual delineation in an apical or basal 4-chamber view at end-diastole and RV FAC was calculated as [(end-diastolic RV area - end-systolic RV area)/end-diastolic RV area]*100. Aortic and pulmonary systolic waves were obtained with angles as close to 0º as possible and velocity-time integrals were calculated by manual trace of the spectral Doppler area under the curve Then, left and right SV were calculated as (π/4*(aortic or pulmonary valve diameter)^2 * (aortic or pulmonary artery systolic flow velocity-time integral)[25]. Cardiac output was calculated as SV*HR[25] and was further adjusted by estimated fetal weight[26]. Left SF was calculated from internal ventricular diameters obtained from a transverse 4-chamber view by M mode using the following equation: [(end-diastolic dimension−end-systolic dimension)/end-diastolic dimension]*100[24]. TAPSE and MAPSE were assessed in an apical or basal 4-chamber view, by applying M-mode to the annular tricuspid and mitral annulus, respectively[27]. Tissue Doppler imaging was used at mitral and tricuspid lateral annuli from an apical or basal 4-chamber view to record S'[28]. RV and LV ejection times were measured from pulmonary and aortic spectral Doppler systolic flow using valves clicks as landmarks. To account for HR differences between subjects, outflow timing measurements were normalized to the cardiac cycle duration and expressed as a percentage of the mean duration of 3 cardiac cycles.

Diastolic function[25] was assessed by ventricular inflow peak velocities in early diastole (E) and atrial contraction (A), E/A ratio and ventricular inflow timings, peak myocardial velocity in early diastole (E') and atrial contraction (A') and early diastolic velocity ratio (E/E'). Right and left ventricular filling was assessed from a basal or apical four-chamber view, placing the pulsed Doppler volume immediately below and in between the tricuspid and mitral valve leaflets, respectivley[29]. E and A transvalvular filling velocities were measured and E/A ratio calculated. RV and LV inflow duration were measured from E-wave onset to A-wave

termination, normalized to the cardiac cycle duration and expressed as a percentage of the mean duration of 3 cardiac cycles. Tissue Doppler imaging was used at mitral and tricuspid lateral annuli from an apical or basal 4-chamber view to record E' and A' myocardial velocities[28] and E/E' ratio was calculated. Significant tricuspid regurgitation was defined as persistent, holosystolic and with regurgitation jet reaching atrial ceiling.

Neonatal echocardiography

Neonatal echocardiography was performed while patients were resting quietly or asleep, using a Philips iE33 XMatrix (Philips Healthcare, Andover, MA, USA) with a 2- to 10-MHz phased-array transducer following a standardized protocol[30]. *Neonatal cardiac morphometric, systolic and diastolic function* measurements were the same as in the fetus, except for RV wall thickness and FAC, which were not obtained in the neonatal assessment.

Synchrotron radiation-based phase-contrast computed tomography

Summarized methods are described. For more details, see the supplementary methods. 3D datasets were obtained using a 20 keV parallel synchrotron X-ray beam. Field of view was 13.03 x 3.2 mm^2 with isotropic pixel size of 5.81µm for the CoA heart and 14 x 9.6 mm^2 with isotropic pixel size of 3.2µm for the normal specimen. Helical angle was computed as the angle between the transverse plane and the vector projection to the local tangential plane of the cylindrical coordinate system of the heart.

Histopathology study

Cardiac histopathology was assessed following standardized institutional protocol. Following paraffin inclusion, representative ventricular cross-sections were stained using

Hematoxilyn-Eosin, Masson's trichrome and Van Giesen stains and the slides were evaluated by an experienced pathologist (CRZ).

Statistical analysis

Data were analyzed using the IBM SPSS Statistics 23 statistical package. Shapiro-Wilk test of normality was performed for continuous variables. Comparisons were performed using Student´s t test, Mann-Whithney U or Wilcoxon W, as appropriate. For simplicity, all continuous variables are presented as median (interquartile range). Categorical variables are presented as percentages and groups were compared using Chi-square test. Case-control baseline characteristics were assessed to identify potential confounders, but no further adjustment was necessary. Bonferroni correction for multiple comparisons was applied.

RESULTS

Study participants

During the study period there were 78 fetuses meeting the inclusion criteria of which 11 opted for termination of pregnancy, 23 were excluded due to pre or postnatal detection of additional major cardiac, extra-cardiac malformations or genetic abnormalities and 1 patient was lost to follow-up (Figure 1). Of the remaining 43 patients, CoA was confirmed postnatally in 30 and ruled out in 13. All CoA cases born in our center during the study period had been prenatally identified and were included in this study. The fetal group consisted of 30 cases with postnatally confirmed CoA, and 60 controls.

Ten newborns with CoA and 16 controls were excluded from postnatal analysis due to prematurity (2 cases and 2 controls), management without PGE1 (2 cases) and incomplete/outside 48-96 hours' time-frame echocardiography (6 cases and 14 controls). Postnatal echocardiography results were, thus, analyzed in 20 CoA cases and 44 controls (Figure 1). All CoA cases included in the postnatal analyses were assessed prior to coarctation treatment.

Baseline and perinatal characteristics

Baseline and perinatal characteristics are shown in Table 1. The study groups were similar in terms of maternal age, GA at scan and estimated fetal weight. Feto-placental Doppler values were normal in both groups.

Both groups were similar in terms of GA at birth, birth weight and pregnancy complications such as prematurity, small for GA and gestational diabetes. No other pregnancy complications were observed. Rates of vaginal delivery were also similar. Low 5-minute Apgar

score was infrequent (2/30 of CoA and none in controls) and umbilical artery pH was normal and similar in both groups. No controls were admitted to the neonatal intensive care unit.

Fetal echocardiography results

Fetal cardiac morphometric and functional characteristics are summarized in Table 2 and Table 3. As expected, there was a right dominance in CoA compared to controls however the dominance was mainly due to smaller left side structures, especially at mid-transverse ventricular diameter. As the long axis lengths were similar, CoA fetuses showed a more elongated LV (increased sphericity index) and a slightly more globular RV (Table 2 and Figure 2). There was no myocardial hypertrophy on either ventricle. Additionally, fetuses with CoA had significantly smaller left atria and larger right atria.

While these morphometric changes were associated with a redistribution of SV and CO in both ventricles (decreased in the LV and increased in the RV), systolic and diastolic functional parameters were preserved, with the exception of increased blood-pool filling velocities (E and A) and a slight increase in E/E' ratio in the LV (Figure 2). Subgroup analysis considering the presence of arch hypoplasia and type of surgical repair did not reveal a different morphometric or functional profile. Fetuses with CoA and ventricular septal defect presented larger left ventricles with similar functional profile to those with intact septum, however the largest filling velocities and E/E' were present in the VSD subgroup (see supplementary results).

Postnatal evolution of CoA cases

Postnatal evolution of the 30 fetal cases is summarized in Table 1. Clinical management of CoA cases was decided in multidisciplinary sessions including neonatologists,

pediatric cardiologists, cardiac surgeons and anesthesiologists and was based on the best available clinical evidence considering the characteristics of the individual patient and the available resources. Twenty-seven patients (90%) were admitted to the neonatal intensive care unit and PGE1 treatment was started in 26 patients (86.7%). Four patients were treated with primary angioplasty including three patients managed without prostaglandin perfusion. Surgery was performed in the remaining patients 26 patients on the 8th day of life (range 2-30 days). Termino-terminal coartectomy was performed in 7 cases while 19 newborns required extended arch repair. Surgical VSD closure was considered necessary in 4/13 patients with VSD. Median age at discharge was 26 days (range 9-103). Major neonatal morbidity was present in 23.3% cases including pneumothorax after chest tube removal, sepsis of abdominal origin, necrotizing enterocolitis and diaphragmatic paralysis.

The 20 cases finally included in postnatal analysis were all admitted to the neonatal intensive care unit and PGE1 treatment was started. Termino-terminal coartectomy was performed in 5 cases and 15 newborns required extended arch repair. The postnatal analysis group included 5 patients with a VSD, of which 1 required surgical closure.

Cardiac histopathological study was performed in the only neonatal death in our fetal study group. This patient, born at 32.4 weeks, died on the 33rd day of life, after coartectomy at 14 days and with clinical recoarctation that required angioplasty on the 27th day. This procedure was complicated by aneurysm development and rupture resulting in massive hemothorax and death. The patient also presented an atrial septal defect with persistent left-to-right shunt leading to progressive right cardiac dilatation, pulmonary hypertension and reduced LV filling. This case was not included in the postnatal echocardiographic analysis due to extreme prematurity.

Neonatal echocardiography results

Neonatal cardiac morphometric and functional characteristics are summarized in Table 4 and Table 5. As in fetal life, newborns with CoA under PGE1 perfusion, showed larger right-to-left ratios, however the ventricular disproportion was less apparent and with no significant differences at the mid-ventricular level. The RV diameters and shape were similar to controls at neonatal assessment. Interestingly, the LV's transverse diameter was similar to controls, and given a shorter length, the LV became significantly more globular in CoA cases (with lower mid-ventricular sphericity index). Additionally, and unlike in fetal life, the left atria were significantly enlarged compared to controls.

After birth, LV CO and SV increased in CoA cases, reaching values similar to controls (Table 4 and Figure 2) while MAPSE and S´ remained similar. LV filling blood-pool velocities (E and A) were significantly increased in CoA with similar E', which translated into a higher E/E' ratio. Additionally, A' was decreased in CoA neonates (Table 5).

RV SV and CO were also higher in CoA newborns, as was the combined cardiac output, which was associated with significantly higher RV early filling velocities (E) and longitudinal systolic and diastolic motion as shown by increased peak annular velocities (E', A' and S'), compared to controls (Table 5).

Myocyte orientation analysis and cardiac histopathology

Figure 3 illustrates the results of the myocyte aggregates orientation analysis performed in the two X-PCI datasets. The architecture of LV myocardium in the two hearts analyzed (one normal and one with CoA) showed the typical gradual change of helical angle (α_H) from epi- to endocardium, with longitudinally aligned fibers (α_H ~ -60º) in the epicardium, more circumferential fibers (α_H ~ 0º) in the midwall and longitudinal fibers (α_H ~ +60º) in the

endocardium, as have been described in the normal adult heart [31], with no evidence of orientation remodeling, myocardial disorganization nor fibrosis in the CoA specimen. Similarly, the available neonatal cardiac histopathology (Figure 4) showed no evidence of myocardial abnormalities nor fibrosis.

DISCUSSION

We provide a comprehensive assessment of biventricular morphometry and function in CoA from fetal to early neonatal life. Fetuses with CoA showed significant left-to-right volume redistribution with RV size and output dominance and significant geometry alterations with an abnormally elongated LV (increased sphericity) and preserved biventricular function and myocardial thickness. Our findings suggest a unique fetal cardiac remodeling in which prenatal volume redistribution avoids LV pressure increase. Postnatally, the LV is acutely volume loaded resulting in an overall geometry change and higher filling velocities.

Our work differs from previous studies, which have focused solely on improving prenatal diagnostic accuracy[3], and provides new insight into the development of the right cardiac dominance in fetuses with CoA and the origin of LV postnatal functional alteration.

Fetal early cardiac remodeling in CoA

Cardiac asymmetry in fetal CoA, often described as right-to-left dominance, resulted from significantly smaller left structures and an abnormally elongated LV shape. The RV was also larger at mid-ventricular level and more globular than in controls (Figure 2). There was no ventricular hypertrophy in either ventricle; additionally, although limited to one specimen, the high-resolution structural data obtained by X-PCI revealed normal myocyte arrangement in CoA (Figure 3). To our knowledge, this is the first study to provide microscopic structural information in the human fetus with CoA, without the artifacts induced by usual histological techniques or contrast agents.

Overall, the elongated shape of the LV, the absence of hypertrophy and of signs of dysfunction are compatible with a functionally normal LV in the setting of decreased LV volume load, further supported by the normal microscopic organization. The volume redistribution

towards the RV allows it to provide most of the lower body flow thus protecting the LV from having to eject volume over the site of CoA, which would result in an additional pressure load.

Thus, the cardiac disproportion present prenatally seems to achieve an optimal ventricular loading balance that limits LV pressure increase, modulated by a reduced right-to-left shunting across the foramen ovale. Animal models support this hypothesis, as right cavities dominance is achieved only by obstructing LV inflow (with an inflated balloon in the left atrium)[32] and not by direct aortic intervention[32,33]. Conversely, maternal hyperoxygenation treatment which increases fetal pulmonary venous return and, thus, LV filling, seems to result in LV growth in CoA fetuses[34]. Also, as seen in our study, VSD presence seems to provide further LV filling and results in larger LVs.

Our findings suggest that, despite biventricular remodeling and CO redistribution, fetuses with CoA have no significant myocardial dysfunction. Although there is limited data on fetal cardiac function in CoA, a few studies report lower LV strain in fetuses with CoA[4,5,35]. These studies initially suggested that the decreased LV strain in CoA fetuses was due to an intrinsically abnormal myocardial differentiation[4]. The argument was based on a postmortem histological study of 13 unoperated heart specimens with hypoplastic/borderline LV associated to CoA[4,36]. However, myocardial histological abnormalities affected only the most severe cases (with multiple left lesions)[36], limiting causality assumptions between isolated CoA and the abnormalities detected. Moreover, it is known that reduced ventricular loading alone results in lower strain without translating ventricular dysfunction[37]. Additionally, increasing LV loading with maternal hyperoxygenation therapy seems to improve LV strain values in CoA fetuses[35]. However, maternal hyperoxygenation therapy on CoA fetuses[34,35] is still in an early stage and future studies will help determine its clinical value. Finally, although limited by sample size, our

synchrotron and histopathology data do not support the hypothesis of an intrinsically abnormal myocardium (Figures 3 and 4).

Early postnatal cardiac adaptation of CoA

Considering our prenatal findings, the LV seems to develop under a low volume-load and normal pressure setting. However, the LV seems unprepared for the acute neonatal volume load, as it shows prompt structural remodeling.

Newborns with CoA quickly normalized the LV CO with an acute LV shape shift towards a globular LV and much increased filling velocities but no signs of restriction. These changes accommodate the increased pulmonary venous return and closed foramen ovale and support systemic flow (Table 4 and 5 and Figure 2).

The only available study in neonates with CoA, prior to surgery and under prostaglandin perfusion, reported LV diastolic alterations and decreased myocardial velocities with normal shortening fraction. These results were obtained at a median age of 15 days (ie. later than in our study), suggesting a progressive maladapted LV response to pressure increase. Additionally, LV impairment seems to persist after surgery[11], and up to 12 years after coartectomy[38], suggesting that LV remains at increased risk of functional impairment. This risk might also be related to the presence of more generalized vascular dysfunction and impaired arterial reactivity[39,40] and might justify the use of afterload reduction therapy in these children after surgery.

At neonatal assessment, RV normalized its size and shape, however, in the context of a patent arterial duct, the RV SV and CO increase persisted, with enhanced longitudinal RV function, as shown by the increased E', A' and S' (Table 5 and Figure 2). Nonetheless, RV functional changes resolve[11] when volume load normalizes after ductal closure.

In the light of our findings, we hypothesize that the prompt LV remodeling results from acute neonatal volume/pressure overload of a previously functionally normal ventricle.

Limitations

The relatively small number of fetuses and the high proportion of cases with VSD might limit the interpretation of results and the power to detect subtle cardiac dysfunction.

Reevaluation of our results in larger cohorts and using different techniques, including strain analysis, as well as a thorough assessment of flow across the foramen ovale, might provide additional information. Further histological and immunohistochemistry analysis of fetal heart specimens with CoA might provide additional information regarding myocardium differentiation, as our analysis is limited to one synchrotron and one histological assessment of CoA hearts.

Conclusions

Fetuses with CoA showed significant left-to-right volume redistribution and associated biventricular remodeling with alterations in size and geometry. These findings suggest a unique fetal cardiac remodeling in which the LV stays smaller from the decreased growth stimulus of reduced volume load. This volume redistribution seems to prevent LV pressure increase. Postnatally, the LV is acutely volume loaded resulting in an overall geometry change, becoming globular but with preserved systolic function. These results improve our understanding of CoA from fetal to neonatal life.

Acknowledgments and funding

We thank the study participants for their personal time and commitment to this project.

This study was supported by grants from Hospital Clinic de Barcelona (Ajut Josep Font, Barcelona, Spain), Fundació Daniel Bravo (Barcelona, Spain), la Caixa Foundation (Barcelona, Spain), Cerebra Foundation for the Brain Injured Child (Carmarthen, Wales, UK), AGAUR 2014 SGR grant nº 928, Instituto de Salud Carlos III (PI14/00226, PI15/00263, PI15/00130 and INT16/00168) as part of the Plan Nacional de I+D+I and co-funded by ISCIII-Subdirección General de Evaluación; the Fondo Europeo de Desarrollo Regional (FEDER) "Otra manera de hacer Europa" (Madrid, Spain); and the Spanish Ministry of Economy and Competitiveness (grant TIN2014-52923-R; Maria de Maeztu Units of Excellence Programme - MDM-2015-0502). We also acknowledge the Paul Scherrer Institut, Villigen, Switzerland for provision of synchrotron radiation beamtime at the TOMCAT beamline X02DA of the SLS and part of this work was carried out with the support of the Diamond Light Source (proposal MT11716). No industry funding was used in the development of this work.

References

1. Rosenthal E. Coarctation of the aorta from fetus to adult: curable condition or life long disease process? *Heart*. 2005;91(11):1495-1502. doi:10.1136/hrt.2004.057182.
2. Wren C, Reinhardt Z, Khawaja K. Twenty-year trends in diagnosis of life-threatening neonatal cardiovascular malformations. *Arch Dis Child Fetal Neonatal Ed*. 2008;93(1):F33-5. doi:10.1136/adc.2007.119032.
3. Familiari A, Morlando M, Khalil A, Sonesson S-E, Scala C, Rizzo G, Del Sordo G, Vassallo C, Elena Flacco M, Manzoli L, Lanzone A, Scambia G, Acharya G, D'Antonio F. Risk Factors for Coarctation of the Aorta on Prenatal UltrasoundClinical Perspective. *Circulation*. 2017;135(8):772-785. doi:10.1161/CIRCULATIONAHA.116.024068.
4. Miranda JO, Hunter L, Tibby S, Sharland G, Miller O, Simpson JM. Myocardial deformation in fetuses with coarctation of the aorta: a case–control study. *Ultrasound Obstet Gynecol*. 2017;49(5):623-629. doi:10.1002/uog.15939.
5. Germanakis I, Matsui H, Gardiner HM. Myocardial Strain Abnormalities in Fetal Congenital Heart Disease Assessed by Speckle Tracking Echocardiography. *Fetal Diagn Ther*. 2012;32(1-2):123-130. doi:10.1159/000334413.
6. Cohn JN, Ferrari R, Sharpe N. Cardiac remodeling-concepts and clinical implications: A consensus paper from an International Forum on Cardiac Remodeling. *J Am Coll Cardiol*. 2000. doi:10.1016/S0735-1097(99)00630-0.
7. Barker DJP. Adult consequences of fetal growth restriction. *Clin Obstet Gynecol*. 2006. doi:10.1097/00003081-200606000-00009.
8. Crispi F, Bijnens B, Figueras F, Bartrons J, Eixarch E, Le Noble F, Ahmed A, Gratacos E. Fetal Growth Restriction Results in Remodeled and Less Efficient Hearts in Children. *Circulation*. 2010;121(22):2427-2436. doi:10.1161/CIRCULATIONAHA.110.937995.

9. García-Otero L, López M, Gómez O, Goncé A, Bennasar M, Martínez JM, Valenzuela-Alcaraz B, Rodriguez-López M, Sitges M, Loncà M, Bijnens B, Crispi F, Gratacós E. Zidovudine treatment in HIV-infected pregnant women is associated with fetal cardiac remodelling. *AIDS*. 2016;30(9):1393-1401. doi:10.1097/QAD.0000000000001066.

10. Guirado L, Crispi F, Masoller N, Bennasar M, Marimon E, Carretero J, Gratacós E, Martínez J, Friedberg M, Gómez O. Biventricular impact of mild to moderate pulmonary valve stenosis in fetal life. *Ultrasound Obstet Gynecol*. March 2017. doi:10.1002/uog.17456.

11. Klitsie LM, Roest AAW, Kuipers IM, Van der Hulst AE, Hazekamp MG, Blom NA, Ten Harkel ADJ. Enhanced Characterization of Ventricular Performance After Coarctation Repair in Neonates and Young Children. *Ann Thorac Surg*. 2013;96(2):629-636. doi:10.1016/j.athoracsur.2013.04.058.

12. Lam Y-Y, Kaya MG, Li W, Gatzoulis MA, Henein MY. Effect of Chronic Afterload Increase on Left Ventricular Myocardial Function in Patients With Congenital Left-Sided Obstructive Lesions. *Am J Cardiol*. 2007;99(11):1582-1587. doi:10.1016/j.amjcard.2007.01.031.

13. Brili S, Tousoulis D, Antoniades C, Aggeli C, Roubelakis A, Papathanasiu S, Stefanadis C. Evidence of vascular dysfunction in young patients with successfully repaired coarctation of aorta. *Atherosclerosis*. 2005;182(1):97-103. doi:10.1016/j.atherosclerosis.2005.01.030.

14. Gonzalez-Tendero A, Zhang C, Balicevic V, Cárdenes R, Loncaric S, Butakoff C, Paun B, Bonnin A, Garcia-Cañadilla P, Muñoz-Moreno E, Gratacós E, Crispi F, Bijnens B, Ardenes RC, Loncaric S, Butakoff C, Paun B, Bonnin A, Garcia-Ca~ Nadilla P, Mu~ Noz-Moreno E, Gratac Os E, Crispi F, Bijnens B. Whole heart detailed and quantitative

anatomy, myofibre structure and vasculature from X-ray phase-contrast synchrotron radiation-based micro computed tomography. *Eur Hear J - Cardiovasc Imaging*. 2017;18(7):732-741. doi:10.1093/ehjci/jew314.

15. Garcia-Canadilla P, Dejea H, Bonnin A, Balicevic V, Loncaric S, Zhang C, Butakoff C, Aguado-Sierra J, Vázquez M, Jackson LH, Stuckey DJ, Rau C, Stampanoni M, Bijnens B, Cook AC. Complex Congenital Heart Disease Associated With Disordered Myocardial Architecture in a Midtrimester Human Fetus. *Circ Cardiovasc Imaging*. 2018;11(10):e007753. doi:10.1161/CIRCIMAGING.118.007753.
16. Robinson HP, Sweet EM, Adam AH. The accuracy of radiological estimates of gestational age using early fetal crown-rump length measurements by ultrasound as a basis for comparison. *Br J Obstet Gynaecol*. 1979;86(7):525-528. http://www.ncbi.nlm.nih.gov/pubmed/476017. Accessed November 9, 2017.
17. Carvalho J, Allan L, Chaoui R, Copel J, DeVore G, Hecher K, Lee W, Munoz H, Paladini D, Tutschek B, Yagel S. ISUOG Practice Guidelines (updated): sonographic screening examination of the fetal heart. *Ultrasound Obstet Gynecol*. 2013;41(3):348-359. doi:10.1002/uog.12403.
18. Bhide A, Acharya G, Bilardo CM, Brezinka C, Cafici D, Hernandez-Andrade E, Kalache K, Kingdom J, Kiserud T, Lee W, Lees C, Leung KY, Malinger G, Mari G, Prefumo F, Sepulveda W, Trudinger B. ISUOG practice guidelines: Use of Doppler ultrasonography in obstetrics. *Ultrasound Obstet Gynecol*. 2013. doi:10.1002/uog.12371.
19. Hadlock FP, Harrist RB, Shah YP, King DE, Park SK, Sharman RS. Estimating fetal age using multiple parameters: A prospective evaluation in a racially mixed population. *Am J Obstet Gynecol*. 1987;156(4):955-957. doi:10.1016/0002-9378(87)90365-6.
20. Figueras F, Meler E, Iraola A, Eixarch E, Coll O, Figueras J, Francis A, Gratacos E,

Gardosi J. Customized birthweight standards for a Spanish population. *Eur J Obstet Gynecol Reprod Biol*. 2008;136(1):20-24. doi:10.1016/j.ejogrb.2006.12.015.

21. García-Otero L, Gómez O, Rodriguez-López M, Torres X, Soveral I, Sepúlveda-Martínez Á, Guirado L, Valenzuela-Alcaraz B, López M, Martínez JM, Gratacós E, Crispi F. Nomograms of Fetal Cardiac Dimensions at 18–41 Weeks of Gestation. *Fetal Diagn Ther*. January 2019:1-12. doi:10.1159/000494838.
22. Paladini D, Chita SK, Allan LD. Prenatal measurement of cardiothoracic ratio in evaluation of heart disease. *Arch Dis Child*. 1990;65(1 Spec No):20-23. doi:10.1136/adc.65.1_Spec_No.20.
23. Schneider C, McCrindle BW, Carvalho JS, Hornberger LK, McCarthy KP, Daubeney PEF. Development of Z -scores for fetal cardiac dimensions from echocardiography. *Ultrasound Obstet Gynecol*. 2005;26(6):599-605. doi:10.1002/uog.2597.
24. DeVore GR, Siassi B, Platt LD. Fetal echocardiography. IV. M-mode assessment of ventricular size and contractility during the second and third trimesters of pregnancy in the normal fetus. *Am J Obstet Gynecol*. 1984;150(8):981-988. doi:10.1016/0002-9378(84)90395-8.
25. Crispi F, Valenzuela-Alcaraz B, Cruz-Lemini M, Gratacós E. Ultrasound assessment of fetal cardiac function. *Australas J Ultrasound Med*. 2013;16(4):158-167. doi:10.1002/j.2205-0140.2013.tb00242.x.
26. Kiserud T, Ebbing C, Kessler J, Rasmussen S. Fetal cardiac output, distribution to the placenta and impact of placental compromise. *Ultrasound Obstet Gynecol*. 2006;28(2):126-136. doi:10.1002/uog.2832.
27. Cruz-Lemini M, Crispi F, Valenzuela-Alcaraz B, Figueras F, Sitges M, Gómez O, Bijnens B, Gratacós E. Value of annular M-mode displacement vs tissue Doppler velocities to

assess cardiac function in intrauterine growth restriction. *Ultrasound Obstet Gynecol*. 2013;42(2):175-181. doi:10.1002/uog.12374.

28. Comas M, Crispi F, Gómez O, Puerto B, Figueras F, Gratacós E. Gestational age- and estimated fetal weight-adjusted reference ranges for myocardial tissue Doppler indices at 24-41 weeks' gestation. *Ultrasound Obstet Gynecol*. 2011;37(1):57-64. doi:10.1002/uog.8870.
29. Hernandez-Andrade E, Benavides-Serralde JA, Cruz-Martinez R, Welsh A, Mancilla-Ramirez J. Evaluation of Conventional Doppler Fetal Cardiac Function Parameters: E/A Ratios, Outflow Tracts, and Myocardial Performance Index. *Fetal Diagn Ther*. 2012;32(1-2):22-29. doi:10.1159/000330792.
30. Lopez L, Colan SD, Frommelt PC, Ensing GJ, Kendall K, Younoszai AK, Lai WW, Geva T. Recommendations for Quantification Methods During the Performance of a Pediatric Echocardiogram: A Report From the Pediatric Measurements Writing Group of the American Society of Echocardiography Pediatric and Congenital Heart Disease Council. *J Am Soc Echocardiogr*. 2010;23(5):465-495. doi:10.1016/j.echo.2010.03.019.
31. Anderson RH, Ho SY, Redmann K, Sanchez-Quintana D, Lunkenheimer PP. The anatomical arrangement of the myocardial cells making up the ventricular mass. *Eur J Cardio-Thoracic Surg*. 2005;28(4):517-525. doi:10.1016/j.ejcts.2005.06.043.
32. Fishman NH, Hof RB, Rudolph AM, Heymann MA. Models of congenital heart disease in fetal lambs. *Circulation*. 1978;58(2):354-364. doi:10.1161/01.CIR.58.2.354.
33. Samson F, Bonnet N, Heimburger M, Rücker-Martin C, Levitsky DO, Mazmanian GM, Mercadier J-J, Serraf A. Left Ventricular Alterations in a Model of Fetal Left Ventricular Overload. *Pediatr Res*. 2000;48(1):43-49. doi:10.1203/00006450-200007000-00010.
34. Zeng S, Zhou J, Peng Q, Deng W, Zhang M, Zhao Y, Wang T, Zhou Q. Sustained

maternal hyperoxygenation improves aortic arch dimensions in fetuses with coarctation. *Sci Rep*. 2016;6(1):39304. doi:10.1038/srep39304.

35. Zeng S, Zhou J, Peng Q, Deng W, Zang M, Wang T, Zhou Q. Sustained Chronic Maternal Hyperoxygenation Increases Myocardial Deformation in Fetuses with a Small Aortic Isthmus at Risk for Coarctation. *J Am Soc Echocardiogr*. 2017;30(10):992-1000. doi:10.1016/j.echo.2017.05.008.
36. Mahtab EAF, Gittenberger-de Groot AC, Vicente-Steijn R, Lie-Venema H, Rijlaarsdam MEB, Hazekamp MG, Bartelings MM. Disturbed myocardial connexin 43 and N-cadherin expressions in hypoplastic left heart syndrome and borderline left ventricle. *J Thorac Cardiovasc Surg*. 2012;144(6):1315-1322. doi:10.1016/j.jtcvs.2012.02.011.
37. Bijnens BH, Cikes M, Claus P, Sutherland GR. Velocity and deformation imaging for the assessment of myocardial dysfunction. *Eur J Echocardiogr*. 2008;10(2):216-226. doi:10.1093/ejechocard/jen323.
38. Florianczyk T, Werner B. Assessment of left ventricular diastolic function in children after successful repair of aortic coarctation. *Clin Res Cardiol*. 2011;100(6):493-499. doi:10.1007/s00392-010-0272-1.
39. Gardiner HM, Celermajer DS, Sorensen KE, Georgakopoulos D, Robinson J, Thomas O, Deanfield JE. Arterial reactivity is significantly impaired in normotensive young adults after successful repair of aortic coarctation in childhood. *Circulation*. 1994;89(4):1745-1750. http://www.ncbi.nlm.nih.gov/pubmed/8149540. Accessed November 9, 2017.
40. de Divitiis M, Pilla C, Kattenhorn M, Zadinello M, Donald A, Leeson P, Wallace S, Redington A, Deanfield JE. Vascular dysfunction after repair of coarctation of the aorta. *Circulation*. 2001;104(suppl 1):I-165-I-170. doi:10.1161/hc37t1.094900.

Figure legends

Figure 1. Flow chart of study participants.

Figure 2. Prenatal and postnatal morphological and functional findings in CoA and controls.
A. Prenatal and postnatal 4-chamber view images and cardiac representation in CoA and controls. The smaller left atrium and the smaller and more elongated LV can be appreciated in the 4-chamber view of the fetus with CoA, as well as the postnatal globular shape. Blood flow redistribution in fetal CoA compared to controls and cardiovascular adaptation to neonatal life are represented adjacent to the 4-chamber view for pre and postnatal CoA and controls.
B. Boxplot graphics and p-values of prenatal (light-grey) and postnatal (dark stripes) left and right mid-ventricular sphericity and stroke volume in CoA and controls.

Figure 3. X-PCI images of fetal CoA (top) specimen and a normal (bottom) heart at 19 weeks showing similar fiber orientation pattern.
A. Virtual longitudinal cuts of the re-sliced X-PCI datasets indicating the short-axis slices in which fiber orientation was measured.
B. Helical angle in fetal CoA (top) and in a normal heart (bottom).

Figure 4. Cardiac histopathology of a newborn with CoA.
A. Low-power microscopic picture of a ventricular cross section (Masson trichrome stain). The left ventricle appears narrower than the right ventricle with no evident hypertrophy.
B. Normal histological myocardium appearance, in a hematoxylin-eosin stain of the LV, with no evidence of myocardial disarray or hypertrophic cardiomyocytes.

Table 1. Perinatal characteristics of the study populations.

	Aortic coarctation (n=30)	**Controls** (n=60)	***p value***
Maternal and feto-placental characteristics			
Maternal age (years)	34.3 (7.9)	32.1 (6.4)	*0.169*
Gestational age at scan (weeks)	33.9 (6.2)	32.9 (3.9)	*0.915*
Estimated fetal weight (g)	2292 (1449)	2184v(887)	*0.919*
Estimated fetal weight centile	70 (47)	52 (47)	*0.266*
Estimated fetal weight < 10th centile	6.7%	3.7%	*0.603*
Umbilical artery PI	1.06 (0.20)	1.00 (0.26)	*0.329*
Median cerebral artery PI	1.74 (0.60)	2.02 (0.36)	*0.064*
Cerebro-placental ratio	1.73 (0.58)	1.96 (0.76)	*0.011*
Cerebro-placental ratio <5th centile	13.3%	5.0%	*0.213*
Delivery outcome			
Vaginal delivery (%)	80.0%	87.1%	*0.508*
Gestational age delivery (weeks)	39.9 (1.71)	39.9 (1.71)	*0.107*
Spontaneous preterm birth < 37 weeks	6.7%	3.6%	*1.000*
Birth weight (g)	3185(704)	3280 (750)	*0.592*
Birth weight < 10th centile	13.3%	10.0%	*0.740*
5-minute Apgar score < 7 (%)	6.7%	0%	*0.119*
Umbilical artery pH	7.26 (0.08)	7.24 (0.09)	*0.260*
Clinical management of aortic coarctation cases			
Admission to NICU (%)	90.0 (27/30)	-	-
Treatment with PGE1 (%)	86.7% (26/30)	-	-
Age at surgery (days)	8.9 ± 5.8	-	-
Length of hospital stay (days)	33.6 ± 16.2	-	-
Major neonatal morbidity (%)	23.3 (7/30)	-	-
Primary angioplasty (%)	13.3 (4/30)	-	-
Termino-terminal coartectomy (%)	23.3 (7/30)	-	-
Extended arch repair (%)	63.3 (19/30)	-	-

PI: pulsatility index, NICU: neonatal intensive care unit.
Data shown as median (interquartile range) or percentage as appropriate.

Table 2. Fetal echocardiography morphometric results in the study populations.

	Aortic coarctation (n=30)	**Controls** (n=60)	***p value***
Gestational age at scan (weeks)	33.9 (6.2)	32.9 (3.9)	*0.915*
Cardiac dimensions			
Cardiac area (cm^2)	11.7 (4.8)	12.5 (4.7)	*0.639*
Cardiac longitudinal diameter (mm)	42.0 (7.1)	41.9 (10.4)	*0.149*
Cardiac transverse diameter (mm)	34.0 (6.1)	34.6 (8.1)	*0.279*
Cardio-thoracic ratio*	0.29 (0.06)	0.27 (0.05)	*0.528*
Cardiac sphericity†	1.2 (0.2)	1.2 (0.2)	*0.612*
Right-left ratios			
Tricuspid/mitral valves ratio	1.5 (0.4)	1.0 (0.2)	*<0.001*
RV/LV mid-transverse diameter ratio	1.6 (0.7)	1.1 (0.3)	*<0.001*
RV/LV longitudinal diameter ratio	1.0 (0.2)	0.96 (0.1)	*0.001*
Pulmonary/aortic valves ratio	1.9 (0.4)	1.1 (0.2)	*<0.001*
Right/left atrial area ratio	1.7 (0.6)	1.1 (0.2)	*<0.001*
RV/LV SV ratio	3.6 (1.9)	1.2 (0.5)	*<0.001*
RV/LV wall thickness ratio	1.0 (0.3)	1.0 (0.2)	*0.233*
Right atrial and ventricular dimensions			
Right atrial area (cm^2)	2.4 (1.3)	1.8 (1.2)	*0.037*
RV longitudinal diameter (mm)	21.4 (6.3)	20.7 (6.3)	*0.177*
RV longitudinal diameter (z-score)	0.4(1.6)	0.02 (1.5)	*0.068*
Tricuspid annulus diameter (mm)	12.9 (2.9)	12.8 (4.9)	*0.262*
Tricuspid annulus diameter (z-score)	0.02 (1.5)	-0.4 (1.6)	*0.085*
RV mid-transverse diameter (mm)	13.4 (4.7)	12.8 (3.9)	*<0.001*
RV mid-transverse diameter (z-score)	1.3 (1.6)	0.3 (1.5)	*<0.001*
Pulmonary valve diameter (mm)	8.3 (2.8)	6.5 (2.1)	*<0.001*
Pulmonary valve diameter (z-score)	1.96 (1.6)	-0.53 (1.6)	*<0.001*
RV basal sphericity‡	1.7 (0.5)	1.6 (0.6)	*0.062*
RV mid sphericity‡	1.5 (0.4)	1.6 (0.4)	*0.001*
Left atrial and ventricular dimensions			
Left atrial area (cm^2)	1.3 (0.6)	1.7 (0.9)	*0.017*
LV longitudinal diameter (mm)	20.4 (5.6)	22.7 (6.9)	*0.438*
LV longitudinal diameter (z-score)	-0.9 (1.5)	-0.45 (1.9)	*0.426*
Mitral annulus (mm)	8.7 (2.3)	11.9 (3.2)	*<0.001*
Mitral annulus (z-score)	-2.5 (1.2)	-0.1 (1.4)	*<0.001*
LV mid-transverse diameter (mm)	8.8 (3.4)	11.8 (3.6)	*<0.001*
LV mid-transverse diameter (z-score)	-1.9 (1.2)	-0.1 (1.5)	*<0.001*
Aortic valve diameter (mm)	4.6 (1.4)	5.9 (1.6)	*<0.001*
Aortic valve diameter (z-score)	-1.27 (1.25)	0.36 (1.9)	*<0.001*
LV basal sphericity‡	2.4 (0.8)	1.8 (0.5)	*<0.001*
LV mid sphericity‡	2.4 (0.7)	1.8 (0.4)	*<0.001*
Myocardial wall thickness			
RV free wall thickness (mm)	3.1 (1.0)	3.5 (1.2)	*0.144*
LV free wall thickness (mm)	3.0 (1.0)	3.3 (1.2)	*0.010*
Septal wall thickness (mm)	3.7 (1.0)	3.4 (0.9)	*0.111*

Data shown as median (interquartile range).

RV=right ventricle, LV= left ventricle. * Cardiothoracic ratio calculated as cardiac/thoracic areas. † Cardiac sphericity calculated as longitudinal/transverse cardiac diameters. ‡ Ventricular sphericity calculated as: longitudinal/transverse (atrio-ventricular valve and mid-transverse diameter).

Table 3. Fetal functional echocardiography results in the study populations.

	Aortic coarctation (n=30)	**Controls** (n=60)	***p value***
Gestational age at scan (weeks)	33.9 (6.2)	32.9 (3.9)	*0.915*
Heart rate (bpm)	137 (9)	138 (17)	*0.567*
Combined cardiac output (ml/min/kg)	450 (195)	436 (176)	*0.040*
Right ventricular function			
Fractional area change (%)	26.1 (13.3)	28.2 (15.9)	*0.855*
Stroke volume (ml)	5.3 (4.0)	3.0 (2.1)	*<0.001*
Cardiac output (L/min)	0.8 (0.6)	0.4 (0.3)	*<0.001*
Cardiac output by EFW (ml/min/kg)	342 (132)	228 (113)	*<0.001*
TAPSE (mm)	7.7 (3.3)	7.6 (2.3)	*0.200*
S' (cm/s)	8.0 (1.3)	7.8 (1.5)	*0.275*
Right ejection time (%)	41.3 (5.1)	42.1 (3.9)	*0.878*
E (cm/s)	42.6 (12.8)	42.0 (12.6)	*0.984*
A (cm/s)	61.4 (16.3)	53.6 (13.8)	*0.250*
E/A	0.7 (0.1)	0.8 (0.1)	*0.734*
Tricuspid inflow time (%)	40.8 (4.8)	40.6 (7.1)	*0.840*
E' (cm/s)	8.3 (1.9)	8.2 (2.1)	*0.114*
A' (cm/s)	12.3 (2.7)	11.2 (3.6)	*0.078*
E/E'	4.9 (1.4)	5.1 (1.5)	*0.552*
Significant tricuspid regurgitation	3.3%	0%	*0.659*
Left ventricle functional parameters			
Stroke volume (ml)	1.7 (0.9)	2.7 (2.8)	*<0.001*
Cardiac output (L/min)	0.2 (0.1)	0.4 (0.4)	*<0.001*
Cardiac output by EFW (ml/min/kg)	107 (53)	192 (100)	*<0.001*
Shortening fraction (%)	40.0 (21.1)	35.5 (12.8)	*0.128*
Ejection fraction (%)	70.7 (25.7)	62.2 (17.1)	*0.064*
MAPSE (mm)	5.0 (1.5)	4.7 (1.4)	*0.968*
S' (cm/s)	7.3 (2.6)	7.1 (1.8)	*0.751*
Left ejection time (%)	40.7 (4.5)	41.1 (4.6)	*0.667*
Isovolumetric contraction time (ms)	40.0 (25)	35.0 (7)	*0.367*
Isovolumetric relaxation time (ms)	52.0 (7)	50.0 (10)	*0.104*
E (cm/s)	43.0 (13.9)	37.0 (11.0)	*0.009*
A (cm/s)	57.7 (13.9)	46.9 (11.5)	*0.001*
E/A	0.8 (0.3)	0.8 (0.2)	*0.325*
Mitral inflow time (%)	42.5 (5.9)	43.2 (6.5)	*0.946*
E' (cm/s)	7.5 (1.7)	7.1 (2.1)	*0.329*
A' (cm/s)	9.2 (1.7)	9.7 (2.8)	*0.651*
E/E'	6.2 (2.1)	5.2 (2.1)	*0.026*

Data shown as median (interquartile range). EFW= estimated fetal weight. TAPSE= tricuspid annular plane systolic excursion. MAPSE= mitral annular plane systolic excursion

Table 4. Neonatal echocardiography morphometric results in the study populations.

	Aortic coarctation (n=20)	**Controls** (n=44)	***p value***
Age at scan (days)	3.0 (1.0)	2.0 (0.8)	*0.283*
Right to left dimensions			
Tricuspid/mitral valves ratio	1.1 (0.4)	1.0 (0.3)	*0.137*
RV/LV mid-transverse diameter ratio	0.9 (0.3)	0.9 (0.2)	*0.837*
RV/LV longitudinal diameter ratio	1.0 (0.2)	0.8 (0.1)	*0.013*
Pulmonary/aortic valves ratio	1.7 (0.5)	1.1 (0.4)	*<0.001*
Right/left atrial area ratio	1.1 (0.3)	1.1 (0.3)	*0.848*
RV/LV SV ratio	2.4 (2.9)	1.4 (1.2)	*0.002*
Right atrial and ventricular dimensions			
Right atrial area (cm^2)	2.6 (1.0)	2.1 (0.4)	*0.010*
RV longitudinal diameter (mm)	25.0 (7.5)	24.0 (4.0)	*0.507*
Tricuspid annulus diameter (mm)	11.3 (4.6)	11.5 (3.0)	*0.471*
RV mid-transverse diameter (mm)	14.3 (3.8)	14.0 (3.0)	*0.205*
Pulmonary valve diameter (mm)	10.0 (1.8)	7.5 (2.5)	*<0.001*
RV basal sphericity*	2.2 (1.0)	2.1 (0.6)	*0.330*
RV mid sphericity*	1.6 (0.4)	1.6 (0.4)	*0.434*
Left atrial and ventricular dimensions			
Left atrial area (cm^2)	2.4 (0.6)	2.0 (0.6)	*0.005*
LV longitudinal diameter (mm)	26.0 (6.5)	28.0 (4.0)	*0.074*
Mitral annulus diameter(mm)	10.0 (2.4)	11.5 (1.8)	*0.001*
LV mid-transverse diameter (mm)	16.0 (3.5)	16.0 (2.8)	*0.649*
Aortic valve diameter (mm)	5.9 (1.3)	7.0 (1.0)	*0.003*
LV basal sphericity*	2.6 (0.8)	2.5 (0.4)	*0.203*
LV mid sphericity*	1.5 (0.4)	1.8 (0.3)	*<0.001*
Wall thickness			
LV free wall thickness (mm)	3.8 (1.2)	3.0 (0.4)	*0.003*
Septal wall thickness (mm)	4.0 (1.6)	3.0 (0.2)	*0.001*
Additional echocardiography findings			
Hypoplastic aortic arch (%)	50%	0%	*<0.001*
Bicuspid aortic valve (%)	27.3%	0%	*<0.001*
Ventricular septal defect (%)	45.5%	0%	*<0.001*
Permeable foramen ovale at scan (%)	13.6%	15.6%	*0.701*

Data shown as median (interquartile range). RV=right ventricle, LV= left ventricle. * Ventricular sphericity calculated as: longitudinal/transverse (atrio-ventricular valve and mid-transverse diameter).

Table 5. Neonatal echocardiography functional results in the study populations.

	Aortic coarctation (n=20)	**Controls** (n=44)	***p value***
Age at scan (days)	3.0 (1.0)	2.0 (0.8)	*0.283*
Heart rate (bpm)	137 (25)	124 (21)	*0.036*
Combined cardiac output (ml/min/kg)	573 (374)	346 (205)	*0.001*
Right ventricular function			
Stroke volume (ml)	9.4 (6.6)	4.0 (4.8)	*0.001*
Cardiac output (L/min)	1.3 (0.8)	0.5 (0.7)	*0.003*
Cardiac output by weight(ml/min/kg)	409 (320)	212 (201)	*0.000*
TAPSE (mm)	9.0 (3.4)	9.0 (3.0)	*0.666*
S' (cm/s)	6.8 (2.1)	5.0 (2.0)	*<0.001*
E (cm/s)	60.5 (47.3)	50.0 (18.0)	*0.020*
A (cm/s)	59.0 (22.3)	62.0 (19.0)	*0.909*
E/A	0.9 (1.0)	0.8 (0.2)	*0.172*
E' (cm/s)	9.3 (6.2)	6.0 (2.0)	*<0.001*
A' (cm/s)	10.1 (4.5)	8.0 (2.4)	*0.003*
E/E'	6.9 (3.2)	7.8 (2.8)	*0.110*
Left ventricular function			
Stroke volume (ml)	3.1 (2.5)	4.2 (1.2)	*0.144*
Cardiac output (L/min)	0.4 (0.3)	0.5 (0.2)	*0.431*
Cardiac output by weight (ml/min/kg)	134 (107)	161 (53)	*0.667*
Shortening fraction (%)	39.1 (13.9)	37.2 (8.8)	*0.066*
MAPSE (mm)	5.4 (3.0)	5.5 (1.0)	*0.889*
S' (cm/s)	4.2 (1.7)	4.0 (2.0)	*0.742*
E (cm/s)	97.0 (55)	57.0 (16.0)	*<0.001*
A (cm/s)	70.5 (24.8)	47.0 (12.0)	*<0.001*
E/A	1.4 (0.6)	1.2 (0.4)	*0.022*
E' (cm/s)	5.2 (2.4)	6.5 (2.0)	*0.357*
A' (cm/s)	4.8 (5.1)	6.0 (3.0)	*0.048*
E/E'	16.8 (12.3)	9.6 (4.7)	*<0.001*

Data shown as median (interquartile range)

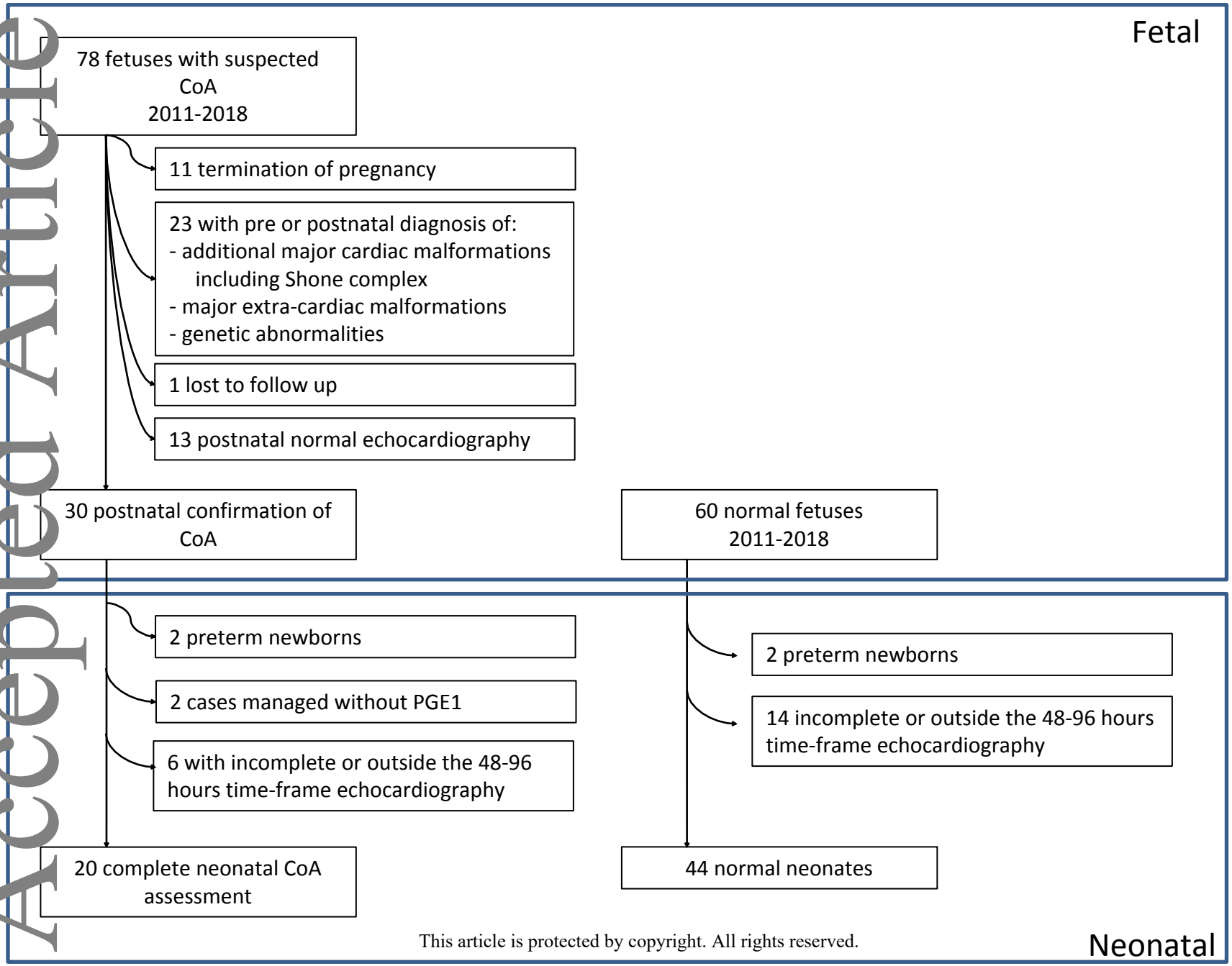

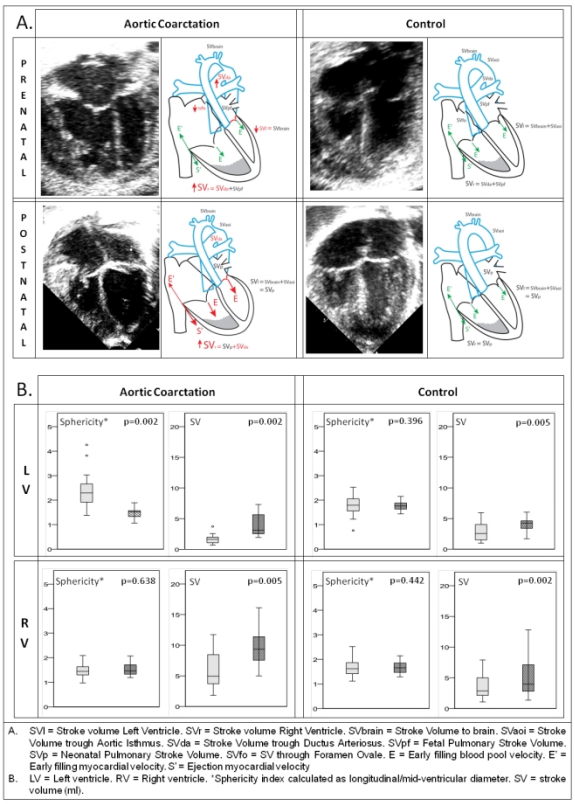

A. SVl = Stroke volume Left Ventricle. SVr = Stroke volume Right Ventricle. SVbrain = Stroke Volume to brain. SVaoi = Stroke Volume trough Aortic Isthmus. SVda = Stroke Volume trough Ductus Arteriosus. SVpf = Fetal Pulmonary Stroke Volume. SVp = Neonatal Pulmonary Stroke Volume. SVfo = SV through Foramen Ovale. E = Early filling blood pool velocity. E' = Early filling myocardial velocity. S' = Ejection myocardial velocity
B. LV = Left ventricle. RV = Right ventricle. *Sphericity index calculated as longitudinal/mid-ventricular diameter. SV = stroke volume (ml).